

Study Characterization of $\text{Co}_{0.3}\text{Zn}_{0.7}\text{Fe}_2\text{O}_4$ Nanoparticles by Co-Precipitation Method within Two Techniques

El-Saaey ASF^{*1}, Khourshid AEFM², Marzouk WW³ and Abdel-Rahman SM¹

¹Mechanical and Electrical Research Institute, National Water Research Centre, Egypt

²Material Engineering Departments, Faculty of Engineering, Tanta University, Egypt

³Production and Design Department, Faculty of Engineering, Minia University, Egypt

Abstract

The $\text{Co}_{0.3}\text{Zn}_{0.7}\text{Fe}_2\text{O}_4$ nanocrystalline synthesized by the Co-precipitation method with two techniques based on different in initial molar concentration (pH suspension). The structural and magnetic properties of the products were determined and characterized in detail by X-ray diffraction (XRD), High Resolution -Transmission Electron Microscope (HR-TEM), Fourier Transform Infrared (FTIR) and vibrating sample magnetometer (VSM). The results suggest the grain size for first technique in the range of 6.14:13 nm and second technique in the range of 8.8:24.4 nm as the calcination temperature increases from 100 to 600°C respectively with different in initial molar concentration (pH suspension) for all techniques. X-ray analysis showed that the samples were cubic spinel structural (kind of inverse spinel oxide). The crystallinity is improved with the increases calcination temperature for all techniques and that proved by the FT-IR and XRD results and compound purity fabricated. HR-TEM analysis showed that nanoparticles size and the shape based on the initial molar concentration (pH suspension) and the calcination temperatures and also indicates that degree of agglomeration for all samples. VSM analysis showed that all the coercivity values were low enough to emphasize that the ferrite was a soft ferrite or super-paramagnetic behavior for most samples.

Keywords: Calcination process; Co-precipitation method; $\text{Co}_{0.3}\text{Zn}_{0.7}\text{Fe}_2\text{O}_4$ Nanoparticles; Ferrite; Magnetic properties

Introduction

Ferrite types with chemical composition variance and the spinel crystal structure are magnetic ceramics (such as Co ferrite, Zn ferrite and Co Zn ferrite) of great importance in the manufacturing of insulators and electronic industrials. The physical, chemical and magnetic properties of ferrite are depends on various parameters such as processing conditions, calcination temperature and time as well as on their chemical composition [1,2]. The properties of these materials mainly depend on their shape, size, and structure, which are strongly determined by the fabrication processes [3,4].

There are several different fabrication techniques used to produce ferrites such as sol-gel, combustion methods, hydrothermal, mechano-chemical and refluxing. However most of them cannot be economically applied on a large scale because they required high vacuum system, complicated experimental steps and high reaction temperatures, but co-precipitation method is considered to be economical technique for ferrite production [5-13].

The aim of the present work is to the synthesis of $\text{Co}_{0.3}\text{Zn}_{0.7}\text{Fe}_2\text{O}_4$ Nanoparticles are prepared by Co-precipitation method with two techniques for its manufactured. The structural and magnetic properties of nano-crystalline cobalt zinc ferrite can be controlled by adjusting the synthesis route in the initial mixtures. The synthesized nano- crystals have been characterized by XRD, HR-TEM, EDX, vibrating sample magnetometer (VSM) and FT-IR, provided below are the investigation details.

Experimental

Materials

All chemical re-agents-ferric chloride FeCl_3 , cobalt(II) chloride CoCl_2 , zinc(II) chloride ZnCl_2 and sodium hydroxide NaOH -were purchased from (El-Gomhouria Co. for Drugs), Egypt and used as received without further treatment.

Instrumentation

X-ray powder diffraction analysis was conducted on a Bruker Axs-D8 Advace Diffractometer (XRD). FTIR transmission spectra were taken on Perkin Elmer Spectrum BX model Infrared Spectrophotometer from 2000 to 400 cm^{-1} . High Resolution- Transmission Electron Microscopy (HR-TEM) analysis was performed on (JEOL 2000FX). Magnetic measurements were carried out with the Quantum Design Model 6000 Vibrating Sample Magnetometer (VSM) and parameters like specific saturation magnetization (M_s), coercive force (H_c) and remanence (M_r) were evaluated.

Procedures

The $\text{Co}_{0.3}\text{Zn}_{0.7}\text{Fe}_2\text{O}_4$ Nanoparticles are prepared by Co-precipitation method with two techniques, So that the Co-precipitation method depends on parameters such as reaction temperature, pH of the suspension, initial molar concentration etc. [14].

In the first and second techniques the mixed solution of CoCl_2 , ZnCl_2 and FeCl_3 in their respective stoichiometry (100 ml of 0.3 M CoCl_2 , 100 ml of 0.7 ZnCl_2 and 100 ml of 2 M FeCl_3) was prepared and kept at 60°C and the preparation of NaOH solution (1 M dissolved in 1200 ml of distilled water), but the difference between two techniques are in first using two burettes for the mix of solution of, CoCl_2 , ZnCl_2

***Corresponding author:** Ahmed Saied Faheim El-Saaey, Mechanical and electrical research institute, National water research Centre, Egypt, Tel: 20244446180; E-mail: Egypt_tech2009@yahoo.com

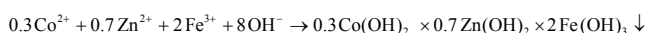
Received October 27, 2016; **Accepted** December 23, 2016; **Published** December 27, 2016

Citation: El-Saaey ASF, Khourshid AEFM, Marzouk WW, Abdel-Rahman SM (2016) Study Characterization of $\text{Co}_{0.3}\text{Zn}_{0.7}\text{Fe}_2\text{O}_4$ Nanoparticles by Co-Precipitation Method within Two Techniques. J Nanomed Nanotechnol 7: 417. doi: 10.4172/2157-7439.1000417

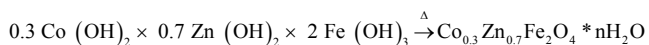
Copyright: © 2016 El-Saaey ASF, et al. This is an open-access article distributed under the terms of the Creative Commons Attribution License, which permits unrestricted use, distribution, and reproduction in any medium, provided the original author and source are credited.

and FeCl_3 and the second burette for NaOH solution in the same time put drops from two burettes in the beaker contains one liter of water within 10 s under constant stirring until pH become 12 as shown in Figure 1a, but in second technique mix of solution of CoCl_2 , ZnCl_2 and FeCl_3 put them in beaker the boiling solution of NaOH was added to the mix of solutions within 10 s under constant stirring until pH become 12 as shown in Figure 1b.

Nano Co Zn ferrites are fabricated by transformation of metal salts into hydroxides. The transformation process occurs immediately, followed by transformation of hydroxides into ferrites. At first solid hydroxides of metals in the form of fine particles were obtained by the co-precipitation of metal cations in alkaline medium (co-precipitation step)



The complex zinc substituted ferrites are obtained by subjecting the solid solution of metal hydroxides to heating in the alkaline medium:



The solutions been preserved at 80°C for 2 h. to transform of hydroxides into spinel ferrite [2,14]. Enough amount of Nanoparticles were collected at this stage by using filtration process under vacuum pressure for samples separation and washing samples several times with distilled water and dried at 100°C temperature and samples subjected for calcination process at 600°C .

Results and Discussions

Physical characterization (XRD analysis)

In Figures 1-4 show the X-ray diffraction patterns of $\text{Co}_{0.3}\text{Zn}_{0.7}\text{Fe}_2\text{O}_4$ nanoparticles samples at 100°C and 600°C . The diffraction patterns show six reflection planes (220), (311), (400), (422), (511), (440) [15]. These clear-cut musings without any confusion, exhibits the formation of a spinel cubic structure and the (hkl) value of the entire peak are which refer to face centered cubic (F.C.C.) structure (kind of inverse spinel oxide). The broad x-ray diffraction peak for the samples for two techniques at 600°C suggest that the ferrite particles are of nano size,

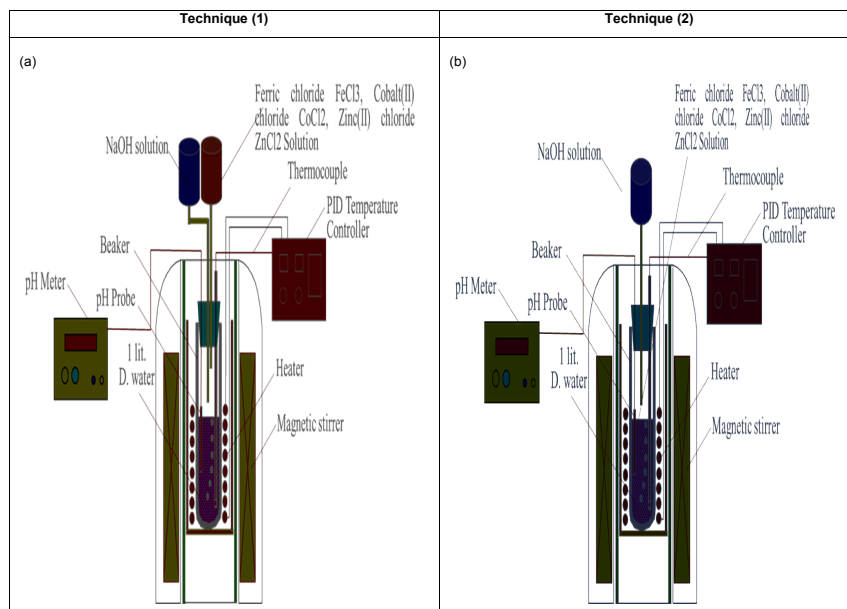


Figure 1: Experimental Setup to $\text{Co}_{0.3}\text{Zn}_{0.7}\text{Fe}_2\text{O}_4$ nanoparticles production.

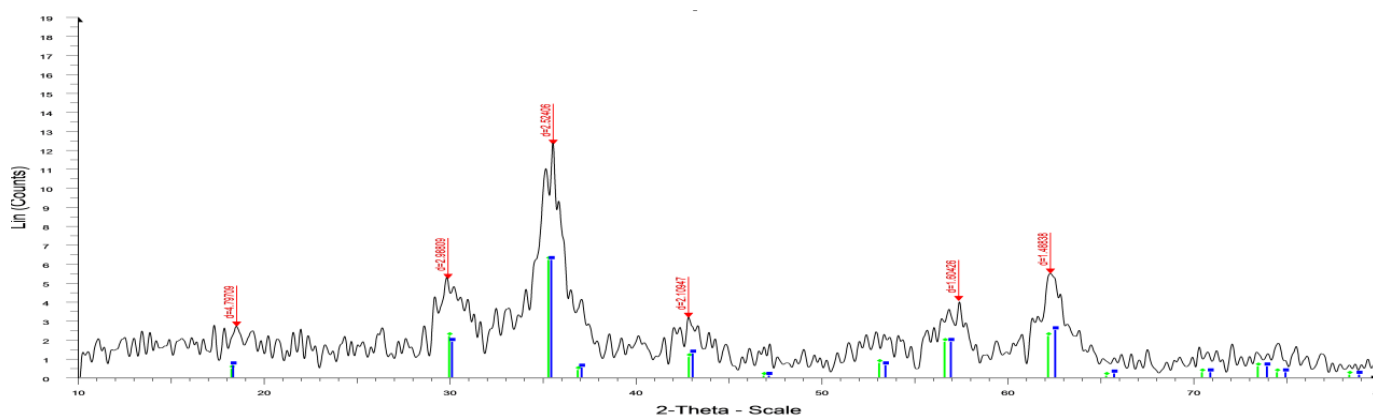


Figure 2: XRD pattern for of $\text{Co}_{0.3}\text{Zn}_{0.7}\text{Fe}_2\text{O}_4$ nanoparticles for 1st technique at 100°C .

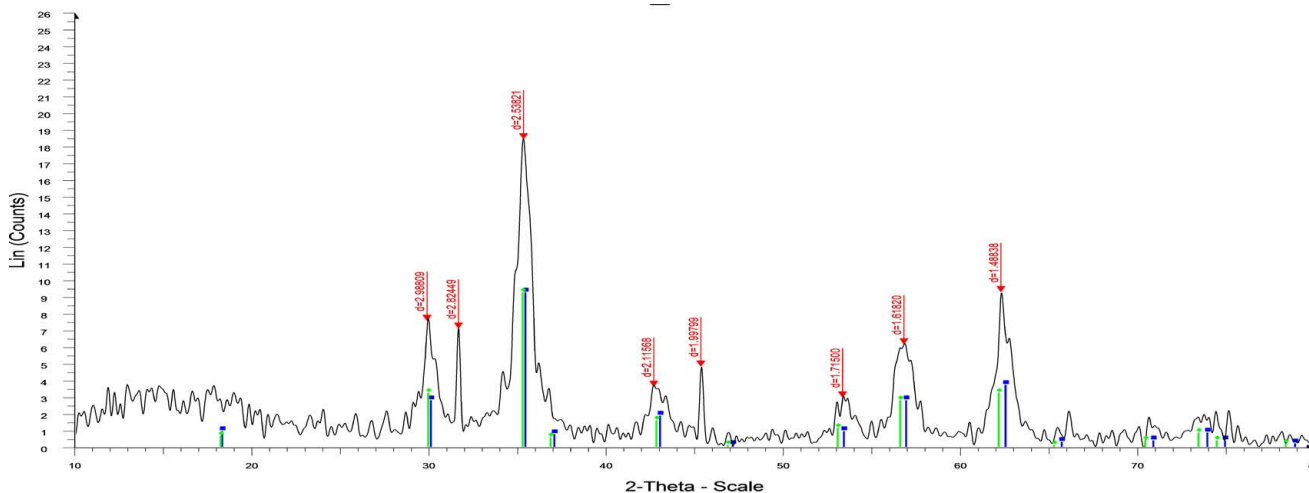


Figure 3: XRD pattern for of $\text{Co}_{0.3}\text{Zn}_{0.7}\text{Fe}_2\text{O}_4$ nanoparticles for 1st technique at 600°C.

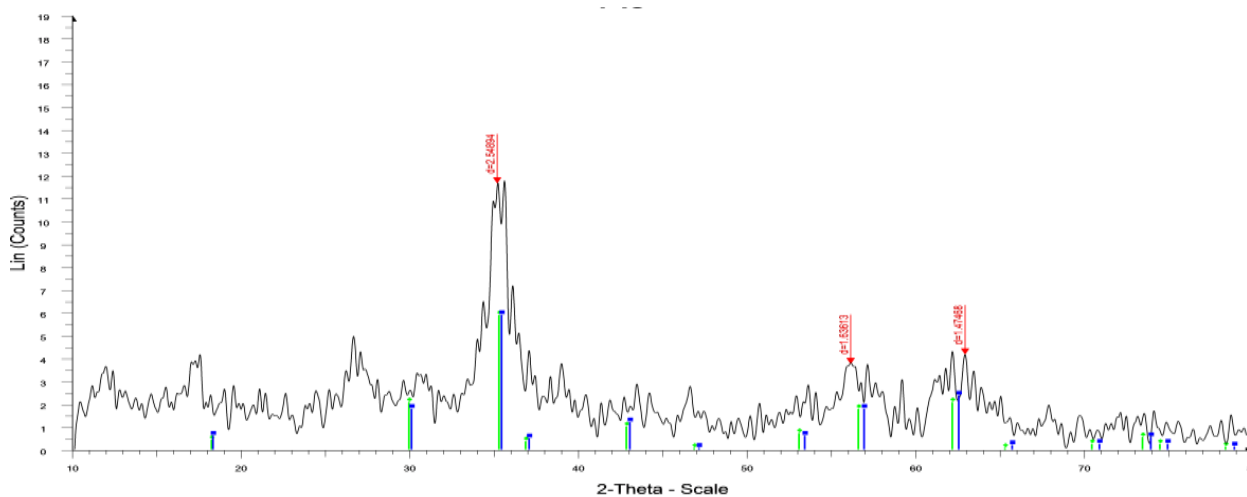


Figure 4: XRD pattern for of $\text{Co}_{0.3}\text{Zn}_{0.7}\text{Fe}_2\text{O}_4$ nanoparticles for 2nd technique at 100°C.

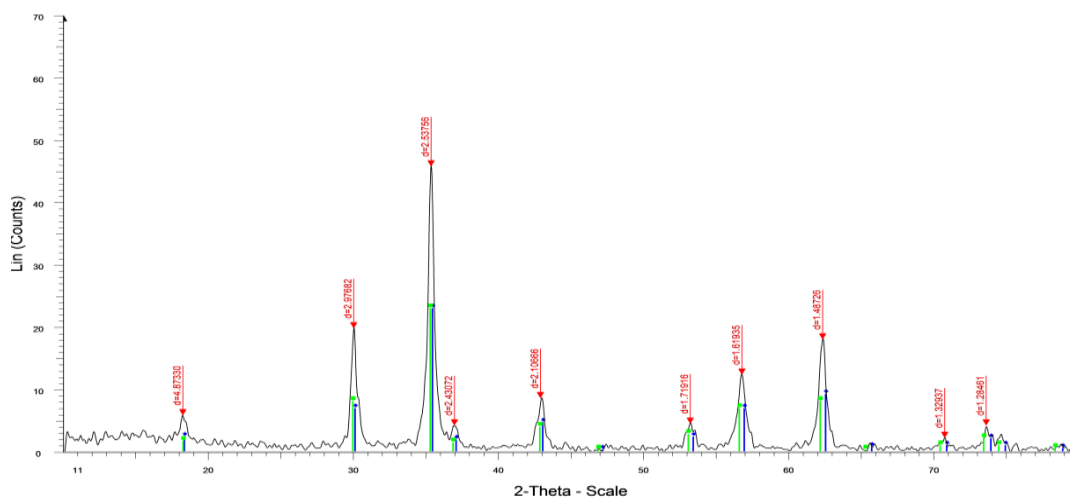


Figure 5: XRD pattern for of $\text{Co}_{0.3}\text{Zn}_{0.7}\text{Fe}_2\text{O}_4$ nanoparticles for 2nd technique at 600°C.

whereas calcination achieve about increase in grain size which leads rise to sharp clear-cut peaks.

The XRD analysis, the average grain size for each samples has been calculated from the XRD line width of the highest intensity peak (311) using Debye Scherrer equation [16], whereas the grain size for first technique in the range of 6.14:13 nm but second technique in the range of 8.8:24.4 nm. In all cases, the grain size decreases with initial molar concentration increased (pH suspension), whereas grain size increases with the increase of calcination temperature. The reduction in grain size can be explained by the particle size effect, more specifically, the effect of surface stress [17].

The initial molar concentration (pH suspension) and calcination parameter with different techniques for sample preparation brought about different changes in the structural properties such as degree of crystallinity, lattice constant, unit cell volume, ionic radii, the distance between the magnetic ions and bond lengths on tetrahedral sites and octahedral sites of cubic spinel structure for each samples [18]. The lattice constant (a_0) can be calculated by Nelson -Riley function and using a least square fit method, whereas the lattice constant for first technique in the range of 8.38:8.51 nm but second technique in the range of 8.42:8.53 nm.

Transmission electron microscope (TEM) measurement and analysis

The Nano-Structure of the $\text{Co}_{0.3}\text{Zn}_{0.7}\text{Fe}_2\text{O}_4$ nanoparticles praperated

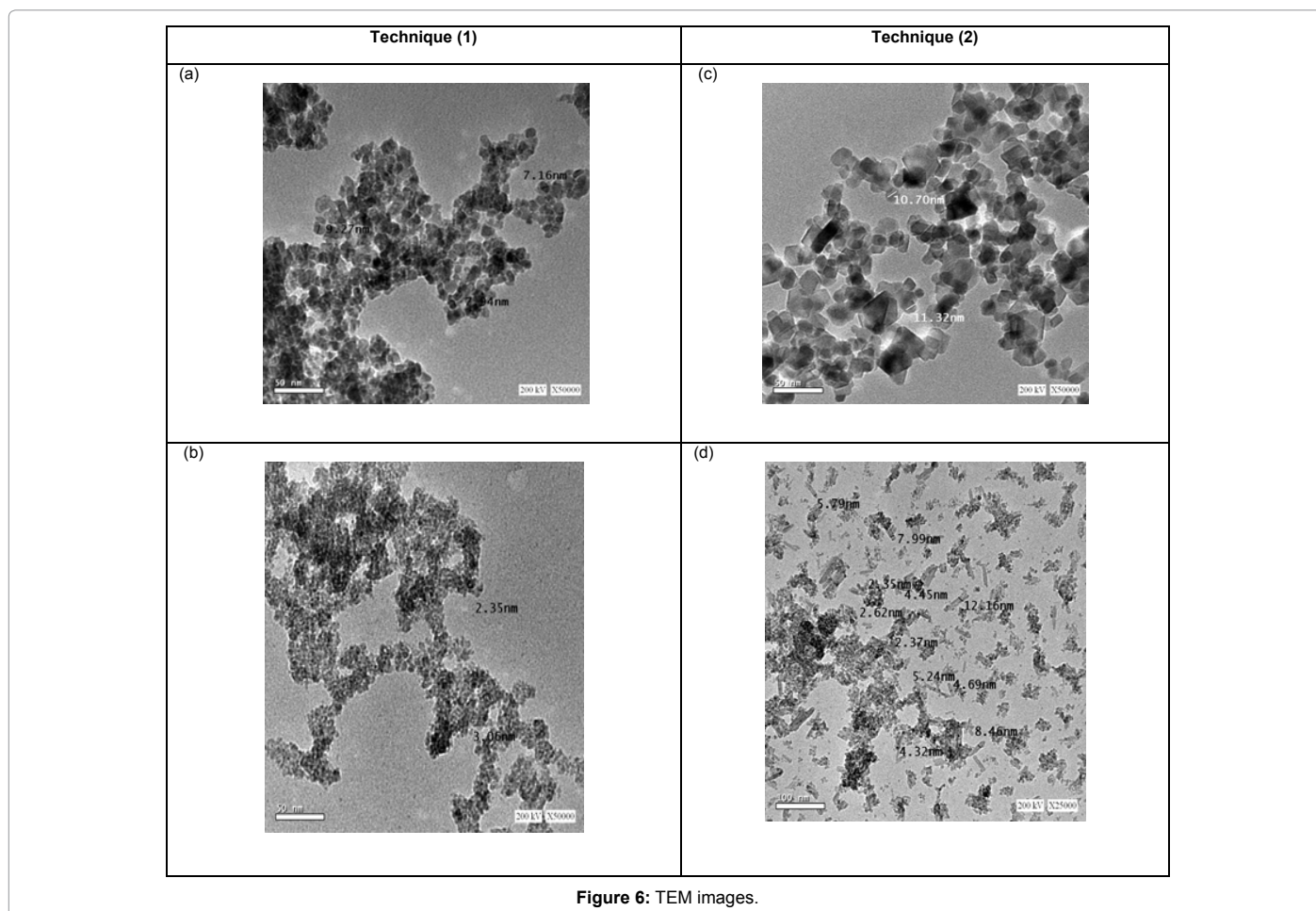
by Co-precipitation method with change in initial molar concentration (pH suspension) and calcination parameter (at 100°C and 600°C), are investigated by HRTEM.

The Figure 5 shows the $\text{Co}_{0.3}\text{Zn}_{0.7}\text{Fe}_2\text{O}_4$ nanoparticles fabrication by two techniques. The first technique Figure 6a and 6b show spherical with uniform size with the calcination temperature increased, but second technique Figure 6c show spherical with uniform size at 100°C, but the calcination temperature increase for same sample at 600°C occurred change in shapes (spherical and rods form) with different size for particles as show in Figure 6d.

Therefore, the HR-TEM results proved the XRD results that appear the nanoparticle size is dependent on the initial molar concentration (pH suspension) and calcination temperature. It is shown that the particles in first technique has a high degree of agglomeration but second technique has a low degree of agglomeration caused by mutual interaction between particles which arises from some parameters such as Vander-walls forces, capillary forces and electrostatic forces. Adding hydroxide solution directly leads to complete the nucleation and growth in a few seconds that effects on agglomeration of particles.

FT-IR analysis

Pradeep and Chandrasekaran are proposed M-O stretching band in ferrites with the frequency bands near 564-588 cm^{-1} and 425-442 cm^{-1} which refer to the tetrahedral and octahedral clusters in ferrites form,



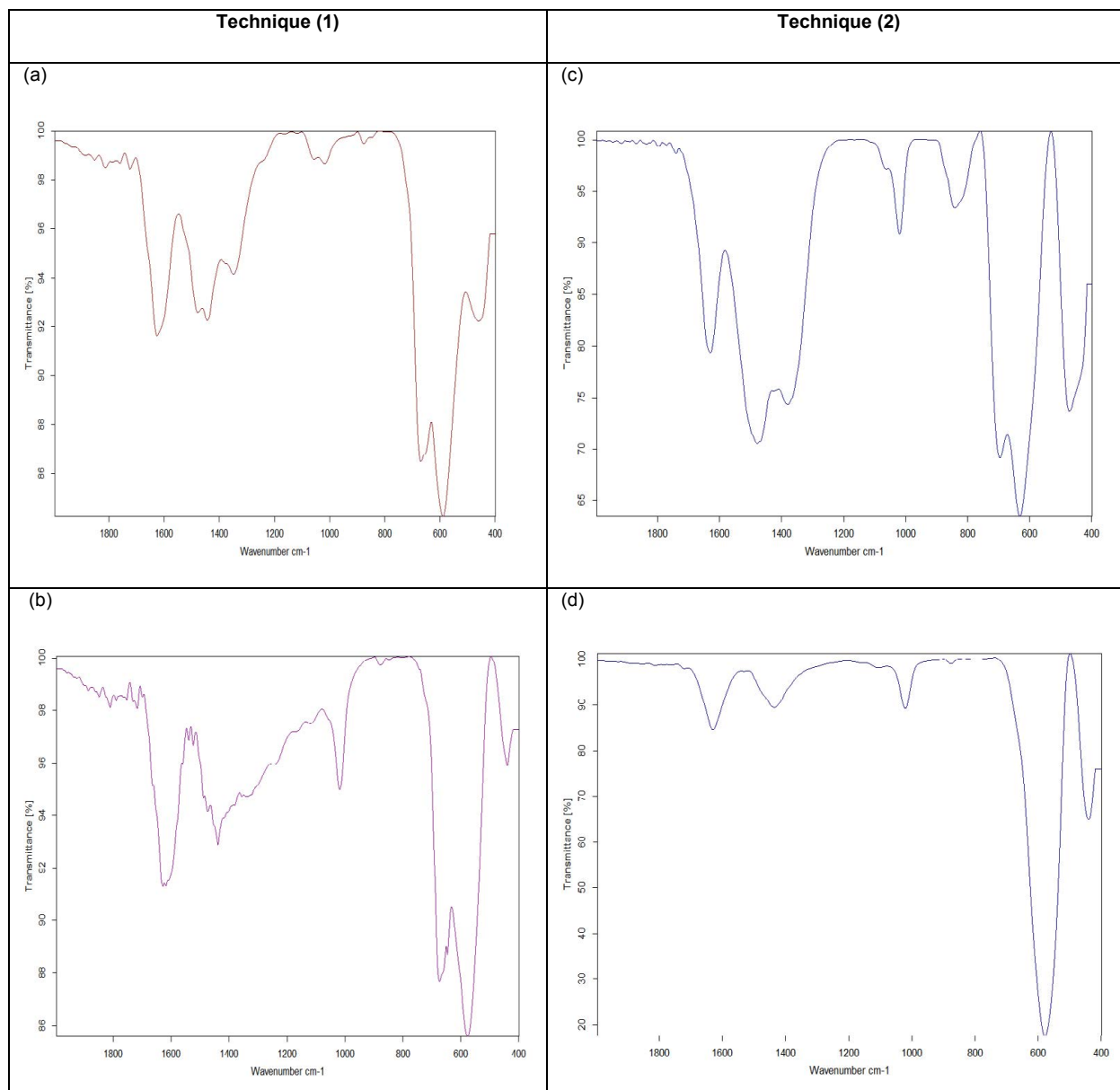


Figure 7: The FTIR absorption bands for two technique.

therefore in Figure 7 show FT-IR analysis are confirms the presence of ferrites phase [19].

The cations distribution analysis for crystal structure in FT-IR spectra are dependent on the vibrational mode of tetrahedral and octahedral clusters but tetrahedral clusters is higher as compared to that of octahedral clusters, which is attributed to the shorter bond length of tetrahedral clusters.

Therefore, FT-IR analysis tool to assess the purity of a compound, from Figure 7 show the FTIR absorption bands for two techniques at room temperature in the wave number range of 400-2000 cm^{-1} It is clear that the higher frequency band is (U1) around 600 cm^{-1} and the lower frequency band (U2) is around 400 cm^{-1} shows that in Figure 7, but in Figure 7d the sample for second technique at 600°C has high purity and degree of crystallinity which confirms the presence spinel

crystal structure. Therefore, the FT-IR results proved the XRD results that appear the cations distribution, crystal structure phase and degree of crystallinity. The highest one corresponds to the intrinsic stretching vibrations of the metal at the tetrahedral site, whereas the U2-lowest band is assigned to octahedral-metal stretching [20,21].

Magnetic properties

Figure 8 shows the hysteresis loop for all samples. Table 1 lists different parameters such as saturation magnetization (M_s), remanent magnetization (M_r), the ratio of remanent magnetization to saturation magnetization (M_r/M_s) and coercivity.

The saturation magnetization for all samples by two techniques produced at 100 C and 600 C is listed in Table 1 where show that the saturation magnetization in first technique increases from 9.6503:17.592 emu/g but in second technique increases from 2.8989 :20.239 emu/g.

Technique	Temp. (°C)	Ms (emu/g)	Mr (emu/g)	Mr/Ms	Coercivity (G)	μ_B (Bohr magneton)
First	100	9.6503	0.19535	0.02	186.09	0.413
	600	17.592	39.043E-3	0.00	11.992	0.753
Second	100	2.8989	99.179E-3	0.03	206.39	0.124
	600	20.239	0.71282	0.03	83.143	0.867

Table 1: Magnetization data of $\text{Co}_{0.3}\text{Zn}_{0.7}\text{Fe}_2\text{O}_4$.

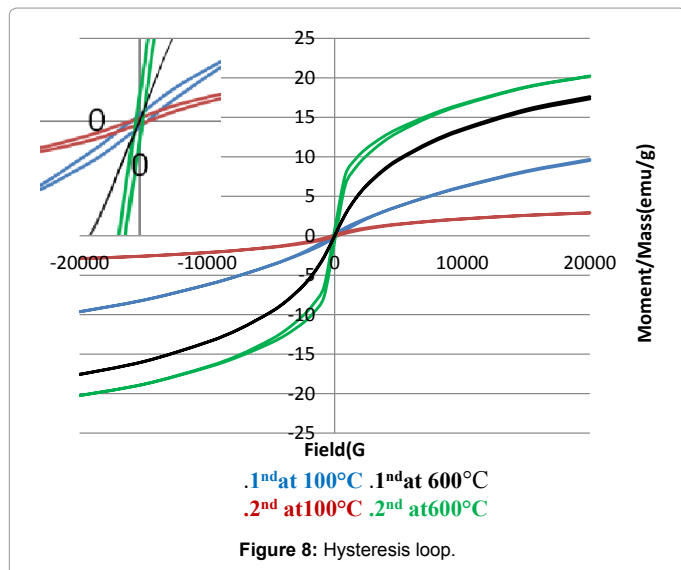


Figure 8: Hysteresis loop.

This may be due to Zn^{2+} (with zero magnetic moment) replacing the ion on the tetrahedral A-sites, causing the decrease of magnetic moment in the sublattice M_A , resulting in the increase of total magnetic moment according to Neel's equation two sublattice model of ferrimagnetism, the magnetic moment per formula unit in μ_B , $n_B N(x)$ is expressed as:

$$n_B N(x) = M_B(X) - M_A(X)$$

Where M_B and M_A are the B- and A-sublattice magnetic moment in μ_B respectively.

Therefore, increase of calcination temperature for samples the saturation magnetization increases. This may be because increase in the lattice parameter, the exchange interaction between A and B sites gets higher resulting in strengthening of A-B interaction and weakening of B-B interaction, which leads to increase of saturation magnetization.

There is a positive relationship between grain size and coercivity H_c in the single domain region according to equation: $H_c = g - \frac{h}{D^2}$, where g and h are constants and 'D' is the diameter of the particle, this may be because of thermal effects. But in the multi-domain region there is an inverse relationship between grain size and coercivity H_c according to equation: $H_c = a + \frac{b}{D}$, where a and b are constants [22-24]. So, the coercivity reduction with increase in the initial molar concentration (pH suspension) and the calcination temperature with two techniques, which can be attributed to the reduction in anisotropy field for all techniques, which in turn reduces the domain wall energy for the first technique less than the second technique. These results refer to the coercivity values reached in the first technique from 186.09 to 11.992 G and the second technique from 206.39 to 83.143 G.

Conclusions

The conclusions can be drawn from the study of $\text{Co}_{0.3}\text{Zn}_{0.7}\text{Fe}_2\text{O}_4$

nanoparticles fabricated by Co-Precipitation method within two techniques as follows:

- The crystallite size depends on the initial molar concentration (pH suspension) and the calcination temperature, where the grain size for the first technique is in the range of 6.14:13 nm but in the second technique the range is 8.8:24.4 nm when the calcination temperature increases from 100 to 600°C respectively.
- The crystallinity of $\text{Co}_{0.3}\text{Zn}_{0.7}\text{Fe}_2\text{O}_4$ nanoparticles might be improved by increasing the calcination temperature, but the crystallinity for the second technique is better than the first technique at 600°C.
- HRTEM indicates a reliance of particle size and shape on the initial molar concentration (pH suspension) and the calcination temperatures. The particle size increases in both techniques, but a nanoparticle has a higher agglomeration degree with the calcination temperature increase in the first technique, but the reverse occurs in the second technique.
- The hysteresis loop shows a reduction in coercivity with the initial molar concentration (pH suspension) and the calcination temperature for all techniques to approximate super-paramagnetic behavior.
- All the coercivity values were low enough to emphasize that the ferrite was a soft ferrite or super-paramagnetic behavior.
- All laboratory results reveal that the initial molar concentration (pH suspension) and the calcination temperature play a major role in changing its structural and magnetic properties significantly.

Acknowledgement

This work was financially supported by the National Water Research Center (NWRC).

References

1. Anderson RD, Griffy KG, Jung D, Door A, Hulse JD, et al. (1995) Ganciclovir absolute bioavailability and steady-state pharmacokinetics after oral administration of two 3000-mg/d dosing regimens in human immunodeficiency virus - and cytomegalovirus - seropositive patients. Clin Ther 17: 425-432.
2. Andrei G, Snoeck, Robert N, Johan S, Marit LM, et al. (2000) Antiviral activity of ganciclovir/valaciclovir acid ester against herpesviruses. Antiviral Res 45: 157-167.
3. Li M, Si L, Pan H, Rabba AK, Yan F, Qiu J, et al. (2011) Excipients enhance intestinal absorption of ganciclovir by P-gp inhibition: assessed in vitro by everted gut sac and in situ by improved intestinal perfusion. Int J Pharm 403: 37-45.
4. Yu CY, Cao H, Zhang XC, Zhou FZ, Cheng SX, et al. (2009) Hybrid nanospheres and vesicles based on pectin as drug carriers. Langmuir 25: 11720-11726.
5. Cordova M, Cheng M, Trejo J, Johnson SJ, Willhite GP, et al. (2008) Delayed HPAM gelation via transient sequestration of chromium in polyelectrolyte complex nanoparticles. Macromol 41: 4398-4404.
6. Ye YJ, Wang Y, Lou KY, Chen YZ, Chen R, et al. (2015) The preparation, characterization, and pharmacokinetic studies of chitosan nanoparticles loaded with paclitaxel/dimethyl- β -cyclodextrin inclusion complexes. Int J Nanomed 10: 4309.

7. Merodio M, Arnedo A, Renedo MJ, Irache JM (2001) Ganciclovir-loaded albumin nanoparticles: characterization and in vitro release properties. *Eur J Pharm Sci* 12: 251-259.
8. Ren J, Zou M, Gao P, Wang Y, Cheng G (2013) Tissue distribution of borneol-modified ganciclovir-loaded solid lipid nanoparticles in mice after intravenous administration. *Eur J Pharma Biopharm* 83: 141-148.
9. Nicolazzi Cl, Venard V, Le Faou A, Finance C (2002) In vitro antiviral efficacy of the ganciclovir complexed with Beta-cyclodextrin on human cytomegalovirus clinical strains. *Antiviral Res* 54: 121-127.
10. Kajiwara E, Kawano K, Hattori Y, Fukushima M, Hayashi K, et al. (2007) Long-circulating liposome-encapsulated ganciclovir enhances the efficacy of HSV-TK suicide gene therapy. *J Control Rel* 120: 104-110.
11. Nagavarma B, Yadav HK, Ayaz A, Vasudha L, Shivakumar H (2012) Different techniques for preparation of polymeric nanoparticles-a review. *Asian J Pharm Clin Res* 5: 16-23.
12. Plapied L, Duhem N, Des RA, Pr eat V (2011) Fate of polymeric nanocarriers for oral drug delivery. *Curr Opin Colloid Interface Sci* 16: 228-237.
13. Belouqui A, Solinis MA, Gascon AR, PozoRodr guez A, Rieux A, et al. (2013) Mechanism of transport of saquinavir-loaded nanostructured lipid carriers across the intestinal barrier. *J Control Rel* 166: 115-123.
14. Calvo P, Remunan LC, Vila JJ, Alonso M (1997) Novel hydrophilic chitosan-polyethylene oxide nanoparticles as protein carriers. *J Appl Polym Sci* 63: 125-132.
15. Calvo P, Remunan LC, Vila JJ, Alonso M (1997) Chitosan and chitosan/ethylene oxide-propylene oxide block copolymer nanoparticles as novel carriers for proteins and vaccines. *Pharm Res* 14: 1431-1436.
16. Egashira K (2007) Pharmaceutical composition containing statin-encapsulated nanoparticle. US Patents 20100086602 A1 2007.
17. Kumari A, Yadav SK, Yadav SC (2010) Biodegradable polymeric nanoparticles based drug delivery systems. *Colloids Surf B* 75: 1-18.
18. Desai MP, Labhasetwar V, Amidon GL, Levy RJ (1996) gastrointestinal uptake of biodegradable microparticles: effect of particle size. *Pharm Res* 13: 1838-1845.
19. Meng J, Sturgis TF, Youan B-BC (2011) Engineering tenofovir loaded chitosan nanoparticles to maximize microbicidemucoadhesion. *EurJPharmSci* 44: 57-67.
20. Elmowafy E, Osman R, El-Shamy AH, Awad G (2014) Stable Colloidal Chitosan/Alginate Nanocomplexes: Fabrication, Formulation Optimization and Repaglinide Loading. *Int J Phar Pharm Sciences* 6: 520-525.
21. Ray M, Pal K, Anis A, Banthia A (2010) Development and characterization of chitosan-based polymeric hydrogel membranes. *Des Monomers Polym* 13: 193-206.
22. Qi L, Xu Z, Jiang X, Hu C, Zou X (2004) Preparation and antibacterial activity of chitosan nanoparticles. *Carbohydr Res* 339: 2693-2700.
23. Bhumkar DR, Pokharkar VB (2006) Studies on effect of pH on cross-linking of chitosan with sodium tripolyphosphate: a technical note. *Aaps Pharmscitech* 7: E138-E43.
24. Dash S, Murthy PN, Nath L, Chowdhury P (2010) Kinetic modeling on drug release from controlled drug delivery systems. *Acta Pol Pharm* 67: 217-223.